

The Detection of a Light Echo from the Type Ia Supernova 2006X in M100

Xiaofeng Wang^{1,2}, Weidong Li¹, Alexei V. Filippenko¹, Ryan J. Foley¹,
Nathan Smith¹, and Lifan Wang³

ABSTRACT

We report the discovery of a light echo (LE) from the Type Ia supernova (SN) 2006X in the nearby galaxy M100. The presence of the LE is supported by analysis of both the *Hubble Space Telescope* (*HST*) Advanced Camera for Surveys (ACS) images and the Keck optical spectrum that we obtained at ~ 300 d after maximum brightness. In the image procedure, both the radial-profile analysis and the point-spread function (PSF) subtraction method resolve significant excess emission at 2–5 ACS pixels ($\sim 0.05'' - 0.13''$) from the center. In particular, the PSF-subtracted ACS images distinctly appear to have an extended, ring-like echo. Due to limitations of the image resolution, we cannot confirm any structure or flux within 2 ACS pixels from the SN. The late-time spectrum of SN 2006X can be reasonably fit with two components: a nebular spectrum of a normal SN Ia and a synthetic LE spectrum. Both image and spectral analysis show a rather blue color for the emission of the LE, suggestive of a small average grain size for the scattering dust. Using the Cepheid distance to M100 of 15.2 Mpc, we find that the dust illuminated by the resolved LE is ~ 27 – 170 pc from the SN. The echo inferred from the nebular spectrum appears to be more luminous than that resolved in the images (at the $\sim 2\sigma$ level), perhaps suggesting the presence of an inner echo at < 2 ACS pixels ($\sim 0.05''$). It is not clear, however, whether this possible local echo was produced by a distinct dust component (i.e., the local circumstellar dust) or by a continuous, larger distribution of dust as with the outer component. Nevertheless, our detection of a significant echo in SN 2006X confirms that this supernova was produced in a dusty environment having small dust particles.

Subject headings: circumstellar matter – dust, extinction – supernovae: general – supernovae: individual (SN 2006X)

1. Introduction

Light echoes (LEs) are produced when light emitted by the explosive outburst of some objects is scattered toward the observer by the foreground or surrounding dust, with delayed arrival time due to the longer light path. This phenomenon is rare, having been observed only around a few variable stars in the Galaxy, and around several extragalactic supernovae (SNe). The best-studied events are SN 1987A (Schaefer 1987; Gouiffes et al. 1988; Chevalier & Emmering 1988; Crotts 1988; Crotts, Kunkel, & McCarthy 1989; Bond et al. 1990; Xu et al. 1995) and the peculiar star V838 Mon (Bond et al. 2003). Other SNe with LEs include

¹Department of Astronomy, University of California, Berkeley, CA 94720-3411, USA; wangxf@astro.berkeley.edu .

²Physics Department and Tsinghua Center for Astrophysics (THCA), Tsinghua University, Beijing, 100084, China; wang_xf@mail.tsinghua.edu.cn .

³Physics Department, Texas A&M University, College Station, TX 77843 .

the Type II SNe 1993J (Liu et al. 2002; Sugerman 2003), 2002hh (Meikle et al. 2006; Welch et al. 2007), and 2003gd (Sugerman 2005; Van Dyk et al. 2006), as well as the Type Ia SNe 1991T (Schmidt et al. 1994; Sparks et al. 1999), 1998bu (Cappellaro et al. 2001; Garnavich et al. 2001), and possibly 1995E (Quinn et al. 2006). Besides their spectacular appearance, LEs offer a unique means to diagnose the composition, distribution, and particle size of the scattering dust. In particular, LEs from the circumstellar environments might provide constraints on SN progenitors.

The Type Ia SN 2006X was discovered on 2006 February 7.10 (UT dates are used throughout this paper) by S. Suzuki and M. Migliardi (IAUC 8667, CBET 393) in the nearby spiral galaxy NGC 4321 (M100). Extensive photometric and spectroscopic coverage is presented by Wang et al. (2007, hereafter W07). They suggest that SN 2006X is highly reddened [$E(B - V)_{\text{host}} = 1.42 \pm 0.04$ mag] by abnormal dust with $R_V = 1.48 \pm 0.06$. Its early-epoch spectra are characterized by strong, high-velocity features of both intermediate-mass and iron-group elements. In addition to the anomalous extinction and the very rapid expansion, SN 2006X exhibits a continuum bluer than that of normal SNe Ia. Moreover, its late-time decline rate in the B band is slow, $\beta = 0.92 \pm 0.05$ mag (100 d) $^{-1}$, significantly below the 1.4 mag (100 d) $^{-1}$ rate observed in normal SNe Ia and comparable to the decay rate of 1.0 mag (100 d) $^{-1}$ expected from $^{56}\text{Co} \rightarrow ^{56}\text{Fe}$ decay. This may suggest additional energy sources besides radioactive decay, such as the interaction of the supernova ejecta with circumstellar material (CSM) and/or a LE.

Attempts to detect the CSM in SNe Ia in different wavebands were unsuccessful before SN 2006X, and only some upper limits could be placed (see Patat et al. 2007a, and references therein) except for the peculiar SNe Ia/IIn 2002ic (Hamuy et al. 2003; Deng et al. 2004; Wang et al. 2004; Wood-Vasey et al. 2004) and 2005gj (Aldering et al. 2006; Prieto et al. 2007). Recent progress in this respect was made from high-resolution spectroscopy by Patat et al. (2007b, hereafter P07), who find time-variable Na I D absorption lines in spectra of SN 2006X. This has been interpreted as the detection of CSM within a few 10^{16} cm (~ 0.01 pc) from the explosion site of the supernova. With the inferred velocity, density, and location of the CSM, P07 proposed that the companion star of the progenitor of SN 2006X is most likely to be a red giant (but see Hachisu et al. 2007, who present a main-sequence star model with mass stripping). Note, however, that SN 2006X exhibited somewhat abnormal features in spectra and photometry; it may not represent a typical SN Ia. Multi-epoch, high-resolution spectral observations of SN 2007af, a normal SN Ia, do not reveal any significant signature of CSM absorption (Simon et al. 2007).

In this paper we report the discovery of an optical LE around SN 2006X, with evidence from *Hubble Space Telescope* (*HST*) Advanced Camera for Surveys (ACS) images and Keck optical spectra. The paper is organized as follows. In §2 we briefly describe the late-epoch data available for SN 2006X, while the data analysis and the interpretation are presented in §3. We discuss the properties of the light echo and the underlying dust in §4. Our conclusions are given in §5.

2. Observations

2.1. *HST* Archival Images

Several epochs of *HST* data covering the site of SN 2006X are publicly available in the MAST archive. The pre-discovery images were taken on 1993 December 31 (Proposal ID 5195: PI, Sparks) by the Wide Field Planetary Camera 2 (WFPC2) in the F439W and F555W filters, with the same integration time of 1800 s. The images taken prior to the SN explosion allow us to examine the immediate environment of the progenitor, whereas the post-explosion observations enable us to search for a possible LE. The most recent,

post-discovery images of SN 2006X were obtained with the High Resolution Channel (HRC, with a mean spatial resolution of $0.026''$ pixel $^{-1}$) of *HST*/ACS on 2006 May 21 (90 d after B maximum) and on 2006 December 25 (308 d after B maximum), respectively (GO-10991; PI, Arlin Crotts). At $t = 90$ d, the SN was imaged in F435W (1480 s), F555W (1080 s), and F775W (1080 s), while at $t = 308$ d, the SN was again observed in the same three bandpasses, with the exposure times of 920 s, 520 s, and 520 s, respectively.

The standard *HST* pipeline was employed to pre-process the images and remove cosmic-ray hits. In Figure 1 we show the pre- and post-explosion *HST* images of SN 2006X in the F555W filter. This pre-discovery image does not reveal any significant source brighter than 24.0 mag in F555W, excluding the possibility of a significant star cluster at the location of SN 2006X. Neither of the two post-discovery images exhibits any resolved LE arcs or rings around SN 2006X. The magnitudes of SN 2006X were measured from the *HST* ACS images with both the Dolphot method (Dolphin 2000) and the Sirianni procedure (Sirianni et al. 2005), and the mean photometry is given in Table 1.

2.2. Keck Optical Spectrum

Observations of nebular-phase spectra provide an alternative way to explore the possibility of an LE around SNe, as the scattered, early-phase light will leave a noticeable imprint on the nebular spectra (e.g., Schmidt et al. 1994; Cappellaro et al. 2001) when the SN becomes dimmer. Two very late-time spectra of SN 2006X taken at $t \approx 277$ and 307 days after B maximum were published by W07 (see their Fig. 19), which were obtained by the Keck telescopes at the W. M. Keck Observatory: one with the Low Resolution Imaging Spectrometer (LRIS; Oke et al. 1995) mounted on the 10 m Keck I telescope, and the other with the Deep Extragalactic Imaging Multi-Object Spectrograph (DEIMOS) mounted on the 10 m Keck II telescope. In the following analysis we focus on the LRIS spectrum taken at $t \approx 277$ d because of its wider wavelength coverage.

3. Data Analysis

3.1. Late-Time Light Curves

Figure 2 shows the absolute B , V , and I light curves of SN 2006X and SN Ia 1996X (Salvo et al. 2001). The former were obtained using the Cepheid distance $\mu = 30.91 \pm 0.14$ mag (Freedman et al. 2001), and corrected for extinction in the Milky Way ($A_V(\text{MW}) = 0.08$ mag; Schlegel et al. 1998) and in the host galaxy ($A_V(\text{host}) = 2.10$ mag; W07). The distance modulus and host-galaxy extinction for SN 1996X are derived by Wang et al. (2006) and Jha et al. (2007) using independent methods, and we adopted the mean values $\mu = 32.11 \pm 0.15$ mag ($H_0 = 72$ km s $^{-1}$ Mpc $^{-1}$ and $A_V(\text{host}) = 0.08$ mag are assumed throughout this paper). The absolute magnitudes of these two SNe are similar near maximum, except in the I band where SN 2006X is ~ 0.4 mag fainter than SN 1996X.

Noticeable differences between the two SNe emerge in B one month after maximum light, when SN 2006X begins to decline slowly at a rate of 0.92 ± 0.05 mag (100 d) $^{-1}$. The discrepancy reaches about 0.9 mag in B at $t = 308$ d, while it is ~ 0.7 mag in V and ~ 0.2 mag in I . This suggests that the emission of SN 2006X is $130\% \pm 60\%$ higher in B , $90\% \pm 40\%$ higher in V , and $20\% \pm 20\%$ higher in I with respect to SN 1996X. The large error bars primarily reflect the uncertainty in the distances.

The apparently overluminous behavior seen in SN 2006X in the tail phase is possibly linked to the light

scattering of the surrounding dust, though the interaction of the SN ejecta with the CSM produced by the progenitor system and/or the excess trapping of photos and positrons (created in $^{56}\text{Co} \rightarrow ^{56}\text{Fe}$ decays within the ejecta) cannot be ruled out. The resultant LE, if present, may not be directly resolved even in the *HST*/ACS images at a distance of ~ 15 Mpc due to the limited angular resolution. To examine this conjecture, in §3.2 we compare the PSFs of the SN and local stars, and in §3.3 we apply the image-subtraction technique to analyze the SN images.

3.2. Radial Brightness Profile

The radial brightness profiles of the images of the SN and local stars in the same field (see Fig. 1) are compared in Figure 3. These were obtained by extracting the flux using different apertures, ranging from 0.1 to 10 pixels with a resolution of 0.1 pixel. The fluxes of the four local stars labeled in Figure 1 are scaled so that the integrated flux within the 10-pixel aperture is the same. Based on the distribution of the radial profiles of these four stars, we derived a mean radial profile with the same integrated flux through Monte Carlo simulations. The radial profile of the four stars was thus normalized by the peak flux of the simulated radial profile.

One can see that the star profiles are uniform at large radius but show noticeable scatter within 2 pixels from the center. For comparison, the central flux of SN 2006X is scaled to be 1.0, with the assumption that the central region of the SN image was not affected by any LE. At $t = 90$ d the SN profile does not show a significant difference from that of the local stars. At $t = 308$ d the SN profiles appear distinctly broader at radii of 2–4 pixels, especially in the F435W and F555W images. Note that the SN data are quite steep at around 1 pixel, probably due to noise.

The inset plot of Figure 3 shows the residual of the radial profile between SN 2006X and the local stars. This was obtained by subtracting the simulated radial profile of the stars from that of the SN. Also plotted is the scatter of the simulated profile of the local stars. At $t = 308$ d, the SN shows significant extra flux in the F435W, F555W, and F775W filters at radii of ~ 2 to 5 pixels, suggesting the presence of a LE. Such a residual flux was not present at $t = 90$ d.

One can see some structure (peaks and valleys) at < 2 pixels in the inset residual plot of Figure 3. These alternating negative/positive residuals clearly show that the substructure within the inner 2 pixels cannot be trusted, and could result from the misalignment of the peak surface brightness of the images. Of course, it is possible that part of the LE is so close to the SN, but the above analysis cannot definitively reveal it.

Integrating the overall residual emission in the range 2–10 pixels, we find that the observed LE brightness is ~ 22.8 mag in F435W, ~ 22.0 mag in F555W, and ~ 22.1 mag in F775W. Its contribution to the total flux of the SN + LE is $\sim 29\%$ in F435W, $\sim 27\%$ in F555W, and $\sim 11\%$ in F775W. In view of potential additional LE emission at radii < 2 pixels, these values are probably lower limits to the true brightness of the LE.

Although Star 1 and SN 2006X show some diffraction spikes in Figure 1, the spikes have the same shape and orientation for all stars in the field. Thus, (a) they should affect the radial surface brightness profiles of all stars in the same way, and not affect the excess light from an echo, and (b) they should be adequately removed by the image subtraction procedure (§3.3).

The difference between the radial profile of SN 2006X and other stars can also be demonstrated by their measured full width at half-maximum intensity (FWHM). Table 2 lists the FWHM of SN 2006X and the

average value of several local stars, obtained by running the IRAF¹ “imexamine” task in three modes: r (radial profile Gaussian fit), j (line 1D Gaussian fit), and k (column 1D Gaussian fit). At $t = 90$ d, the PSF of SN 2006X is comparable to that of the average values of the local stars, while at $t = 308$ d, the SN exhibits a significantly broader profile. The FWHM increases by about 0.3 pixel in the r -profile and by ~ 1.0 pixel in the j -profile and k -profile with respect to the local stars. The reasonable interpretation is that the PSF is broadened by scattered radiation (that is, the LE).

3.3. Light Echo Images

The radial-profile study suggests the presence of a LE in SN 2006X. In this section, we apply image subtraction to provide further evidence for the LE, and study its two-dimensional (2D) structure.

We extract a small section (20×20 pixels) centered on SN 2006X and Star 1 (the brightest star in the field), and align their peak pixels to high precision (0.01 pixel). We then scale Star 1 so that its peak has the same counts as that of SN 2006X, and subtract it from the SN 2006X image. The underlying assumption is the same as in our radial-profile study: the central peak of SN 2006X is not affected by any LE.

Figure 4 shows the PSF-subtracted images of SN 2006X. The left panel shows the subtracted images at the original *HST*/ACS resolution. To bring out more details, the middle panel shows subsampled images by using a cubic spline function to interpolate one pixel into 8×8 pixels. The right panel has three circles (with radii of 2, 4, and 6 pixels, respectively) overplotted. The residual images all show an extended, bright, ring-like feature around the supernova, consistent with the general expected appearance of a LE. These features emerge primarily at radii of 2–4 pixels (or $0.05''$ – $0.11''$) in the images, consistent with those derived above from the radial profiles. The central structure seen within a circle of radius 2 pixels (e.g., the asymmetric feature in F435W, the double features in F775W, and the arc in F555W) are not to be trusted; due to the limited spatial resolution, the images used for the image subtraction may not be perfectly aligned (in terms of the geometry and/or the flux of the central regions), and some artifacts could be introduced at the center of the subtracted images. Similarly, the apparent clumps within the echo ring are not reliable, generally being only a few pixels in size.

The integrated flux, measured from the PSF-subtracted images at 2–10 pixels from the SN site, contributes to the total flux of SN + LE by $\sim 33\%$ in F435W, $\sim 29\%$ in F555W, and $\sim 9\%$ in F775W. This is fully consistent with the above estimate from the radial-profile analysis, taking into account the uncertainty in the PSF subtraction. The brightness of the LE component is estimated to be ~ 22.7 mag in F435W, ~ 21.9 mag in F555W, and ~ 22.3 mag in F775W.

As with the radial-profile analysis, the PSF-subtraction method might remove some fraction of flux from the LE itself; it had been assumed that none of the flux in the central 2-pixel radius is produced by the LE, but this might be incorrect. Thus, our estimate of the echo flux from the image analysis may be only a lower limit of the true LE emission. In view of the image analysis, we cannot verify or rule out that the LE may be distributed continuously from the SN site to an angular radius of ~ 6 pixels ($0.15''$).

¹IRAF, the Image Reduction and Analysis Facility, is distributed by the National Optical Astronomy Observatory, which is operated by the Association of Universities for Research in Astronomy, Inc. (AURA) under cooperative agreement with the National Science Foundation (NSF).

3.4. Light Echo Spectrum

A consistency check for the existence of a LE around a source can also be obtained by comparing the observed supernova spectrum and the synthetic spectrum using an echo model. The observed spectrum should be a combination of the intrinsic late-time SN spectrum and the early-time scattered SN spectrum. Inspection of the late-epoch Keck spectrum (see Fig. 19 of W07) clearly reveals that SN 2006X behaves unlike a normal SN Ia, showing a rather blue continuum at short wavelengths and a broad absorption feature near 6100 Å (probably due to Si II λ 6355).

To construct the composite spectrum containing the echo component, we use the nebular-phase spectrum of SN 1996X to approximate that of SN 2006X. SN 1996X is a normal SN Ia in the elliptical galaxy NGC 5061 (Salvo et al. 2001), with $\Delta m_{15} = 1.30 \pm 0.05$ mag, similar to that of SN 2006X (W07). Late-time optical spectra with wide wavelength coverage and high signal-to-noise ratio (S/N) are available on day 298 for SN 1996X (Salvo et al. 2001; <http://bruford.nhn.ou.edu/~suspect/>) and on day 277 for SN 2006X (W07). Comparing the spectrum of SN 2006X obtained at $t = 277$ d with that taken at $t = 307$ d, we found that the overall spectral slope changed little during this period. We thus could extrapolate the original nebular spectra $t = 308$ d, a phase when both SNe have relatively good multicolor photometry. To completely match the spectrum of SN 2006X, the spectral flux of SN 1996X was multiplied by a factor of 3.0 caused by the difference in distances. Extinction corrections have also been applied to the nebular spectra of these two SNe (W07; Wang et al. 2006).

We considered the cases of both SN 2006X and SN 1996X as the central pulse source when deriving the echo spectrum. The observed spectra of SN 2006X are available at eleven different epochs from about -1 d to 75 d after B maximum, while 14 spectra of SN 1996X are available from about -4 d to 87 d after B maximum (Salvo et al. 2001). The above spectra were properly dereddened² and interpolated to achieve uniform phase coverage. Regardless of the original flux calibration, all of the input spectra have been recalibrated according to their light curves at comparable phases (W07; Salvo et al. 2001) and corrected for the effects of scattering using a similar function, $S(\lambda) \propto \lambda^{-\alpha}$ (e.g., Suntzeff et al. 1988; Cappellaro et al. 2001). These corrected spectra were then coadded and scaled, together with the nebular spectrum of SN 1996X, to match the nebular spectrum of SN 2006X.

The best-fit α values obtained for the combinations of SN 2006X (near B maximum) + SN 1996X (nebular) and SN 1996X (near B maximum) + SN 1996X (nebular) are 3.0 ± 0.3 and 3.3 ± 0.5 , respectively. One can see that the combination of SN 2006X + SN 1996X gives a somewhat better fit to the observed spectrum of SN 2006X. This is not surprising; the spectrum of SN 2006X differs from that of a normal SN Ia at early times, showing extremely broad and blueshifted absorption minima (W07). The large value of α may indicate a small grain size for the scattering dust. The composite nebular spectrum and the underlying echo spectrum are compared with the observed spectrum of SN 2006X in Figure 5 (upper and middle panels). Given the simple assumption of the scattering function, incomplete spectral coverage, and intrinsic spectral difference between SN 1996X and SN 2006X, the agreement between the observation and the model is satisfactory, with major features in the spectrum well matched. This provides independent, strong evidence for the LE scenario. However, the broad emission peak seen at $\lambda \approx 4300\text{--}4500$ Å cannot be reasonably fit by the echo model (see Fig. 5); this mismatch is probably produced by intrinsic features in the nebular spectrum of SN 2006X.

²Here we assume that the dust surrounding SN 2006X is a plane-parallel slab and/or shell, so that both the SN and the LE were affected by roughly the same amount of extinction.

3.5. Light-Echo Luminosity and Color

We can constrain the properties of the LE and the underlying dust through the luminosity and colors of the LE. The LE luminosity of SN 2006X has been estimated by analyzing the *HST* SN images; it can also be obtained by integrating the echo spectrum shown in Figure 5. The magnitudes of the echo given by different methods are listed in Table 3. For the image-based measurement, the error accounts only for the scatter of the stellar PSF. On the other hand, for the spectrum-based measurement, the error primarily consists of the uncertainties in extinction correction (i.e., ~ 0.2 mag for SN 2006X and ~ 0.1 mag for SN 1996X in the B band) and distance modulus (i.e., ~ 0.14 mag for SN 2006X and ~ 0.15 mag for SN 1996X).

We note that the echo inferred from the spectral fitting seems somewhat brighter than that revealed by the image analysis: $\delta m_{F435W} = -0.6 \pm 0.3$ mag. This difference is also demonstrated in the bottom panel of Figure 5, where the flux ratio of the inferred echo spectrum and the observed spectrum of SN 2006X is plotted as a function of wavelength. Overplotted are the ratios yielded for the photometry of the echo image (circles) and the spectrophotometry of the echo spectrum (squares) in F435W and F555W, respectively. Such a discrepancy, at a confidence level of only $\sim 2\sigma$, may suggest that there is some echo emission within a radius of 2 pixels ($21\% \pm 12\%$ of the total flux of SN + LE in F435W and $17\% \pm 11\%$ in F555W) that was not resolved by the image analysis. Despite this possibility, we must point out that the echo luminosity derived from the echo spectrum may have an error that is actually larger than our estimate, since we did not consider possible uncertainties associated with the spectrum itself and the simple scattering model adopted in our analysis (see §3.4).

Assuming that all of the observed differences between the light curves and spectra of SN 2006X and SN 1996X at $t = 308$ d are entirely due to the LE around SN 2006X, we can place an upper limit on the LE brightness as 21.9 ± 0.3 mag in F435W and 21.3 ± 0.3 mag in F555W. The magnitudes and the resulting color are not inconsistent with those presented in Table 3, especially in the case of the spectral fit which likely takes into account most of the echo emission. This leaves little room for other possible mechanisms for the extra emission, suggesting that the echo is the primary cause of the abnormal overluminosity of SN 2006X at $t = 308$ d.

We find, from analysis of both the *HST* images and the nebular spectrum (see Table 3), that the LE has an average color $(F435W-F555W)_{\text{echo}} = 0.8 \pm 0.3$ mag (this roughly equals $(B - V)_{\text{echo}} = 0.8 \pm 0.3$ mag), which is much bluer than the SN color at maximum brightness. The LE is clearly brighter in bluer passbands than at redder wavelengths (see Fig. 5). Comparing the colors of the echo and the underlying SN light helps us interpret the dust, as the color shift depends on the scattering coefficient and hence on the dimensions of the dust grains (Sugerman 2003a).

Integrating over the entire SN light curve (W07) from about -11 d to 116 d after B maximum yields $(B - V)_{\text{SN}} = 1.70$ mag for the overall emission of SN 2006X. The observed change in color, $\Delta(B - V) = -0.9 \pm 0.3$ mag, is much larger than the color shift derived for Galactic dust but is comparable to the change derived for Rayleighian dust³, $\Delta(B - V)_{\text{max}} = -0.96$ mag (Sugerman et al. 2003b). This is consistent with constraints from the direct spectral fit, which suggests that the dust has a scattering efficiency proportional to $\lambda^{-3.0}$. We thus propose that the dust surrounding SN 2006X is different from that of the Galaxy and may have small-size grains, perhaps with diameter $\lesssim 0.01 \mu\text{m}$, reflecting the shorter wavelengths of light more effectively. Smaller dust particles are also consistent with the low value of $\Re_V \approx 1.5$ derived by W07.

³The Rayleighian dust consists of only small particles with grain size $< 0.01 \mu\text{m}$, and hence has a scattering efficiency proportional to λ^{-4} (Sugerman 2003a).

3.6. Dust Distance

Of interest is the distribution of the dust producing the echo; for example, it may be a plane-parallel dust slab or a spherical dust shell. Couderc (1939) was the first to correctly interpret the LE ring observed around Nova Persei 1901. Detailed descriptions of LE geometries can also be found in more recent papers (e.g., Sugerman 2003a; Tytenda et al. 2004; Patat 2005). In general, the analytical treatment shows that both a dust slab and a dust shell could produce an echo that is a circular ring containing the source. Assuming that the SN light is an instantaneous pulse, then the geometry of an LE is straightforward: the distance of the illuminated dust material lying on the paraboloid can be approximated as

$$R \approx \frac{D^2\theta^2 \mp (ct)^2}{2ct}, \quad (1)$$

where D is the distance from the SN to the observer, θ is the angular radius of the echo, c is the speed of light, and t is the time since the outburst. The equation with a minus sign corresponds to the single dust slab, while the plus sign represents the case for a dust shell.

As suggested by the analysis of the radial profile and the PSF-subtracted image of the SN, there is a confirmed LE ring $\sim 0.08''$ away from the SN, with a possible width of $\sim 0.03''$. For this echo of SN 2006X, $ct = 0.27$ pc, which leads to $R \approx 27\text{--}120$ pc, consistent with the scale of the ISM dust cloud. As the dust cloud in front of SN 2006X seems to be very extended, we do not give the thickness of the dust along the line of sight. Considering the possible echo emission within 2.0 pixel ($\sim 0.05''$) inferred from the echo luminosity (see discussion in §4.1) and that extending up to 5 pixels ($\sim 0.13''$; see Fig. 3), the actual distribution of the dust may be from <27 pc to ~ 170 pc from the SN.

In principle, one can also estimate the distance of the dust itself from the SN through a fit to the observed echo luminosity using the light-echo model (e.g., Cappellaro et al. 2001), as the actual echo flux is related to the light emitted by the SN, the physical nature of the dust, and the dust geometry. However, current analytical treatments for the LE model must assume some idealized configuration, which may not apply to the dust surrounding SN 2006X that is found to probably have smaller dust grains with $\mathcal{R}_V \approx 1.5$ and a relatively extended distribution. Moreover, multiple scattering processes rather than a single scattering should be considered in the echo model due to the large optical depth measured from the dust: $\tau_d^V \approx 2.0$ for SN 2006X. Detailed modelling of the LE emission seen in SN 2006X is beyond the scope of this paper.

4. Discussion

Analysis of both the late-time *HST* images and the late-time Keck optical spectrum favors the presence of a LE in SN 2006X, the fourth non-historical SN Ia with a detection of echo emission. Comparison of the SN 2006X echo with the other three known events, SNe 1991T, 1995E, and 1998bu, shows that the Type Ia echoes may have a wide range of dust distances from $\lesssim 10$ pc to ~ 210 pc. The echo detected in SN 1991T is consistent with being a dust cloud of radius 50 pc (Sparks et al. 1999), while the echo speculated from SN 1995E probably corresponds to a dust sheet at a distance of 207 ± 35 pc (Quinn et al. 2006). Garnavich et al. (2001) proposed from the *HST* WFPC2 imaging that SN 1998bu may have two echoes, caused by dust at 120 ± 15 pc and < 10 pc away from the SN; the outer echo is consistent with an ISM dust sheet, while the inner component is likely from the CSM dust. On the other hand, the resolved echo image of SN 2006X appears quite extended in the direction perpendicular to the line of sight. This yields a dust distance spanning from ~ 27 pc to ~ 170 pc away from the site of the SN, indicating that the dust causing the LE

may not be a thin dust sheet but could be a cloud or shell distribution of the dust around the progenitor or a more complicated dust system.

The echo from SN 2006X is found to be brighter than that of the other three Type Ia echo events. Assuming the echo magnitude listed in Table 3 and the SN peak magnitude derived in W07, one can find that the echo flux with respect to the extinction-corrected peak magnitude of SN 2006X is ~ 9.6 mag in V . Quinn et al. (2006) proposed that all of the other three Type Ia echoes (SNe 1991T, 1995E, 1998bu) show a striking similarity in their echo brightness relative to the extinction-corrected peak SN brightness, $\Delta V \approx 10.7$ mag. According to the analytical expression of the dust scattering (e.g., Patat 2005), the excess echo brightness from SN 2006X by ~ 1 mag perhaps suggests a dust distribution closer to the SN, given the similar optical depth for SNe 2006X and 1995E. The SN 2006X echo emission also shows a prominent wavelength dependence, with more light from the shorter wavelengths, suggestive of smaller-size dust around SN 2006X. This is also demonstrated by the difference of the scattering coefficient α required to fit the observed nebular spectrum, which is ~ 3.0 for SN 2006X, ~ 2.0 for 1991T (Schmidt et al. 1994), and ~ 1.0 for SN 1998bu (Cappellaro et al. 2001).

In fitting the nebular spectrum, the echo brightness is found to be $\sim 60\%$ brighter than that from the echo image at the $\sim 2\sigma$ level, likely suggesting the presence of a local echo that was not resolved at the regions close to the SN site. Regarding the location of the echo emission in SN 2006X, one may naturally tie the distribution of the dust underlying the echo to a combination of local CSM dust and distant ISM dust, given the quite extended dust distribution and the small dust grains that were not typical for the ISM dust. Detection of the CSM dust is of particular importance for understanding SN Ia progenitor models. P07 recently reported the detection of CSM in SN 2006X from variable Na I D lines, and they estimate that the absorbing dust is a few 10^{16} cm from the SN. It is hence expected that an echo very close to the SN (< 0.01 pc away) should be produced, although the SN UV radiation field could destroy or change the distribution of the surrounding dust particles out to a radius of a few 10^{17} cm (Dwek 1983). However, it is not possible for us to detect the emission of such a close CSM echo at $t = 308$ d, since the maximum delayed travel time of the light for this echo is < 0.1 yr and the SN radiation decreases with time.

As noted by W07, the spectrum of SN 2006X probably showed a UV excess at $t \approx 30$ d. This may be a signature of the nearby CSM claimed by P07, but the S/N of the spectrum is quite low below 4000 \AA . In this case, the possible echo emission at < 27 pc inferred from the nebular spectrum at $t = 308$ d could result from a dust shell that is farther out than that claimed by P07. This is possible if the CSM dust around SN 2006X has multiple shells, such as the dust ring (or shell) of a planetary nebula (Wang 2005) and nova-like shells.

The presence of a local echo helps explain the slow decline of the B -band light curve of SN 2006X at early phases. Nevertheless, the local echo (if present) is not necessarily from the CSM dust, as forward scattering from the distant dust cloud in front of the SN could also produce an echo of very small angular size. To further distinguish between the two possible cases of distant ISM plus local dust and single ISM dust, future *HST* observations of SN 2006X are necessary. More late-phase *HST*/ACS images would help constrain the evolution of the LE. Using equation (1), we can predict the evolution of the echo ring with time. If the dust formed as a result of past mass loss from the central source, the echo will be more symmetric and the expansion will slow down after the initially rapid phase; with time, its size will eventually shrink to zero. On the other hand, if the dust is of interstellar origin, the echo should expand continuously with slowly decreasing brightness as more-distant regions are illuminated. Assuming that the inner component of the echo within 2 pixels is caused by a CSM dust shell ~ 1 pc from the SN, then the emission within 2 pixels will finally decrease to zero at $t \approx 6.5$ yr. In contrast, the local echo from distant ISM dust should remain

nearly constant for a longer time.

It is worth pointing out that the recent nearby SNe Ia, SN 2007gi (CBET 1017, CBET 1021), SN 2007le (CBET 1100, CBET 1101), and probably SN 2007sr (CBET 1172,1174, ATEL 1343), may exhibit high-velocity features in their spectra similar to those of SN 2006X. If the SN 2006X-like events preferentially occur in environments with abundant ISM dust or CSM dust (Wang et al. 2008, in prep.), then we might expect to detect late-time echo emission in the above three SNe Ia. Thus, it would be interesting to obtain future high-resolution *HST*/ACS images of these SNe.

5. Conclusions

The emergence of a LE in SN 2006X has been confirmed with PSF-subtracted *HST* ACS images which show a ring-like, but rather extended, echo 2–5 pixels (0.05''–0.13'') from the SN site at $t = 308$ d past maximum brightness. A Keck nebular spectrum of the SN taken at a similar phase provides additional evidence for the LE scenario; it can be decomposed into a nebular spectrum of a normal SN Ia and a reflection spectrum consisting of the SN light emitted at early phases.

From the resolved echo image, we derive that the intervening dust is ~ 27 –170 pc from the supernova. Based on the quite blue color of the echo, we suggest that the mean grain size of the scattering dust is substantially smaller than Galactic dust. Smaller dust particles are also consistent with the low \mathcal{R}_V value obtained from the SN photometry. Our detection of a LE in SN 2006X confirms that this SN Ia occurred in a dusty environment with atypical dust properties, as suggested by the photometry (W07).

Analysis of the nebular spectrum might also suggest a local echo at < 27 pc (or at < 2 pixels) that is not resolved in the PSF-subtracted image. This possible local echo is likely associated with the CSM dust produced by the progenitors, though detailed modeling of the echo spectrum and/or further high-resolution imaging are required to test for the other possibilities, such as very forward scattering by a distant cloud or CSM-ejecta interaction.

Some of the data presented herein were obtained at the W. M. Keck Observatory, which is operated as a scientific partnership among the California Institute of Technology, the University of California, and the National Aeronautics and Space Administration (NASA). The Observatory was made possible by the generous financial support of the W. M. Keck Foundation. This research was supported by NASA/*HST* grants AR–10952 and AR–11248 from the Space Telescope Science Institute, which is operated by the Association of Universities for Research in Astronomy, Inc., under NASA contract NAS5–26555. We also received financial assistance from NSF grant AST–0607485, the TABASGO Foundation, the National Natural Science Foundation of China (grant 10673007), and the Basic Research Funding at Tsinghua University (JCqn2005036).

REFERENCES

- Aldering, G., et al. 2006, *ApJ*, 650, 510
 Bloom, J. S., et al. 2007, *ATEL*, 1343
 Bond, H. E., Gilmozzi, R., Meakes, M. G., & Panagia, N. 1990, *ApJ*, 354, L49

- Bond, H. E., et al. 2003, *Nature*, 422, 405
- Cappellaro, E., et al. 2001, *ApJ*, 549, L215
- Chevalier, R. A., & Emmering, R. T. 1988, *ApJ*, 338, 388
- Couderc, P. 1939, *Ann. Astrophys.*, 2, 271
- Crotts, A. 1988, *ApJ*, 333, L51
- Crotts, A. P. A., Kunkel, W. E., & McCarthy, P. J. 1989, *ApJ*, 347, L61
- Deng, J. S., et al. 2004, *ApJ*, 605, L37
- Dolphin, A. E. 2000, *PASP*, 112, 1383
- Drake, A. J., et al. 2007, *CBET*, 1172
- Dwek, E. 1983, *ApJ*, 274, 175 *ApJ*, 558, 323
- Hachisu, I., Kato, M., & Nomoto, K. 2007, *ApJ*, submitted (arXiv:0710.0319)
- Harutyunyan, A., Benetti, S., & Cappellaro, E. 2007, *CBET* 1021 1941, *AJ*, 93, 70
- Garnavich, P., et al. 2001, *AAS*, 199, 4701
- Gouiffes, C., et al. 1988, *A&A*, 198, L9
- Filippenko, A. V., Silverman, J. M., Foley, R. J., & Modjaz, M. 2007, *CBET* 1101
- Freedman, W. L., et al. 2001, *ApJ*, 553, 47
- Jha, S., Riess, A. G., & Kirshner, R. P. 2007, *ApJ*, 659, 122
- Kotak, R., et al. 2004, *MNRAS*, 354, L13
- Liu, J. F., Bregman, J. N., & Seitzer, P. 2003, *ApJ*, 582, 919
- Mathis, J. S., Rumpl, W., & Nordsieck, K. H. 1977, *ApJ*, 217, 425
- Meikle, W. P. S., et al. 2006, *ApJ*, 649, 332
- Monard, L. A. G. 2007, *CBET* 1100
- Nakano, S. 2007, *CBET* 1017 Meixner, M. 2004, *AJ*, 128, 2339
- Patat, F. 2005, *MNRAS*, 357, 1161
- Patat, F., et al. 2007a, *A&A*, 474, 931
- Patat, F. 2007b, *Science*, 317, 924 (P07)
- Prieto, J. L., et al. 2007, *ApJ*, submitted (arXiv:0706.4088)
- Quinn, J. L., et al. 2006, *ApJ*, 652, 512
- Salvo, M. E., et al. 2001, *MNRAS*, 321, 254

- Schlegel, D. J., Finkbeiner, D. P., & Davis, M. 1998, *ApJ*, 500, 525
- Schaefer, B. E. 1987, *ApJ*, 323, L47
- Schmidt, B. P., et al. 1994, *ApJ*, 434, L19
- Sirianni, M., et al. 2005, *PASP*, 117, 1049
- Simon, J. D., et al. 2007, *ApJ*, 671, L25
- Suzuki, S., & Migliardi, M. 2006, *IAUC* 8667
- Sparks, W. B., Macchetto, F., Panagia, N., Boffi, F. R., Branch, D., Hazen, M. L., & Della Valle, M. 1999, *ApJ*, 523, 585
- Suntzeff, N. B., et al. 1988, *Nature*, 334, 135
- Sugerman, B. E. K., & Crofts A. P. S. 2003a, *ApJ*, 632, L17
- Sugerman, B. E. K. 2003b, *AJ*, 126, 1939
- Sugerman, B. E. K. 2005, *ApJ*, 632, L17
- Tylenda, R. 2004, *A&A*, 414, 223
- Umbriaco, G., et al. 2007, *CBET*, 1174
- Van Dyk, S. D., Li, W., & Filippenko, A. V. 2006, *PASP*, 118, 351
- Wang, L. F., et al. 2004, *ApJ*, 604, L53
- Wang, L. F. 2005, *ApJ*, 635, L33
- Wang, X. F., et al. 2006, *ApJ*, 645, 488
- Wang, X. F., et al. 2007, *ApJ*, in press (arXiv:0708.0140)(W07)
- Welch, D. L., et al. 2007, *ApJ*, 669, 525
- Wood-Vasey, W. M., et al. 2004, *ApJ*, 616, 339
- Xu, J., et al. 1994, *ApJ*, 435, 274

Table 1: Late-Time *HST* Photometry of SN 2006X.^a

UT Date	JD–2,450,000	Phase (d)	F435W	F555W	F775W
05/21/2006	3876.0	+90.0	18.71(04)	17.36(02)	16.46(02)
12/25/2006	4094.0	+308.0	21.48(06)	20.56(09)	19.69(02)

^aUncertainties in hundredths of a magnitude are given in parentheses.

Table 2: FWHM of SN 2006X and Local Stars in *HST* Images.

Object	r (pixel)	j (pixel)	k (pixel)	bandpass
$t = 90$ d				
SN	2.21	2.61	2.51	F435W
star	2.17±0.02	2.60±0.03	2.60±0.05	F435W
SN	2.38	2.70	2.68	F555W
star	2.39±0.05	2.81±0.04	2.78±0.03	F555W
SN	2.79	2.84	2.85	F775W
star	2.82±0.05	2.89±0.08	2.89±0.03	F775W
$t = 308$ d				
SN	2.50	3.85	3.36	F435W
star	2.21±0.03	2.81±0.03	2.51±0.02	F435W
SN	2.62	4.00	3.69	F555W
star	2.33±0.03	2.74±0.02	2.64±0.05	F555W
SN	2.95	3.37	3.33	F775W
star	2.79±0.01	2.94±0.02	2.83±0.02	F775W

Table 3: Light Echo of SN 2006X at $t = 308$ d

Method	F435W (mag)	F555W (mag)	F775W (mag)
Residual radial profile (2–10 pixels)	22.8±0.1	22.0±0.3	22.1±0.7
PSF-subtracted image (2–10 pixels)	22.7±0.1	21.9±0.3	22.3±0.9
Synthetic echo spectrum (SN 1996X)	22.2±0.3	21.4±0.3	...
Synthetic echo spectrum (SN 2006X)	22.1±0.3	21.5±0.3	...

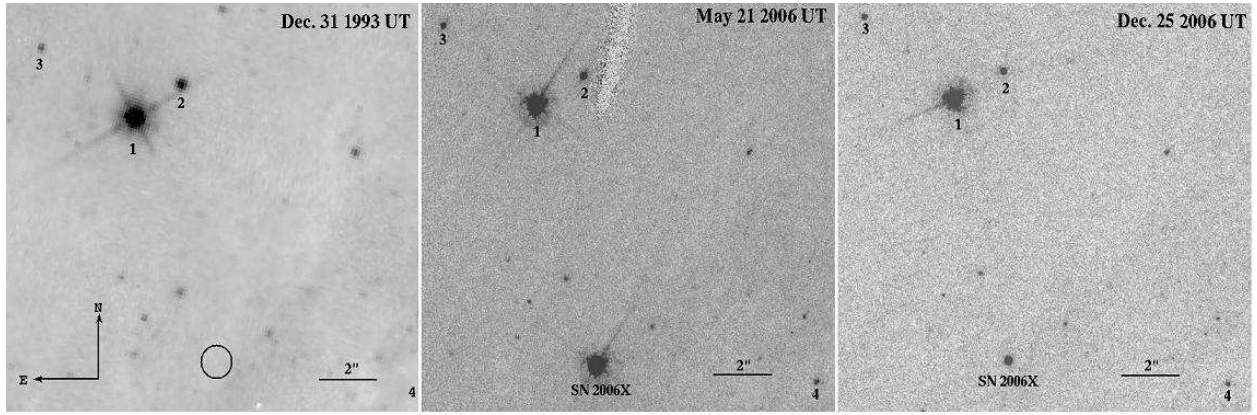


Fig. 1.— (Left) An *HST* image of SN 2006X in the F555W band, taken on 1993 December 31; the circle marks the position of the SN. (Middle) The same field was imaged on 2006 May 21 (90 d after *B* maximum). (Right) The same field was observed on 2006 December 25 (308 d after *B* maximum). The supernova and the reference stars are labeled.

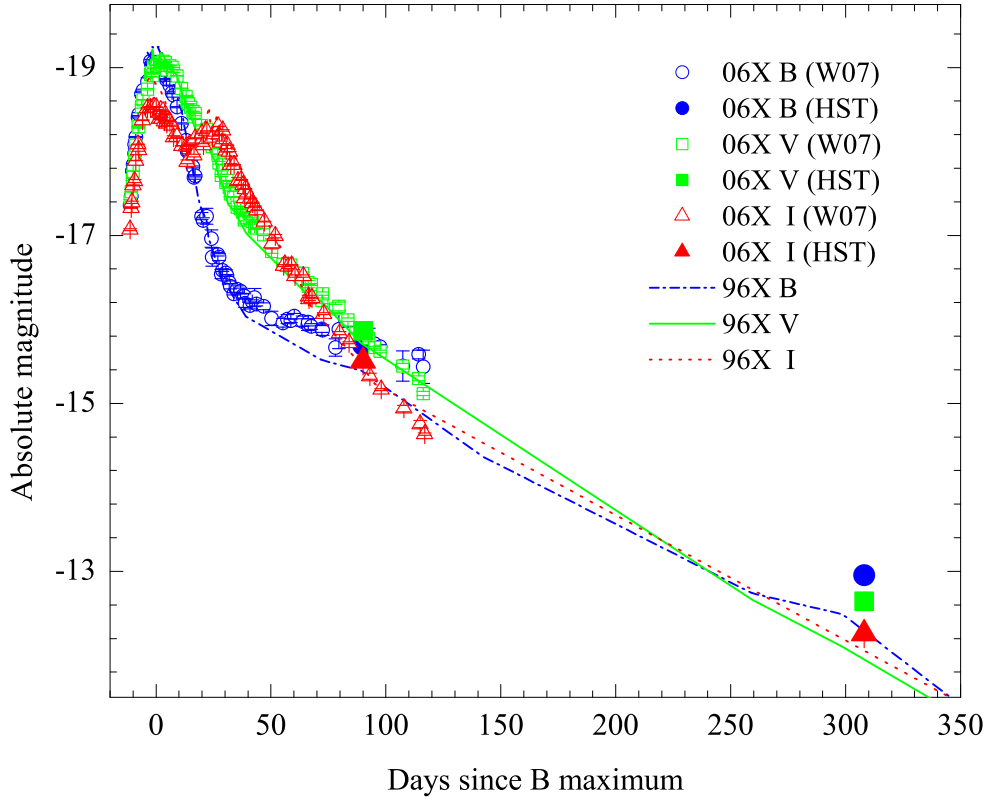


Fig. 2.— Light curve of SN 2006X (symbols) compared with that of SN Ia 1996X (dashed lines). The open circles represent the B , V , and I data from Wang et al. (2007). The filled circles denote the *HST* magnitudes that were transformed from the F435W, F555W, and F775W bands (see Table 1) to the B , V , and I bands (respectively) through an empirical correlation (Sirianni et al. 2005). Proper extinction corrections have been applied to all of the magnitudes (see text for details).

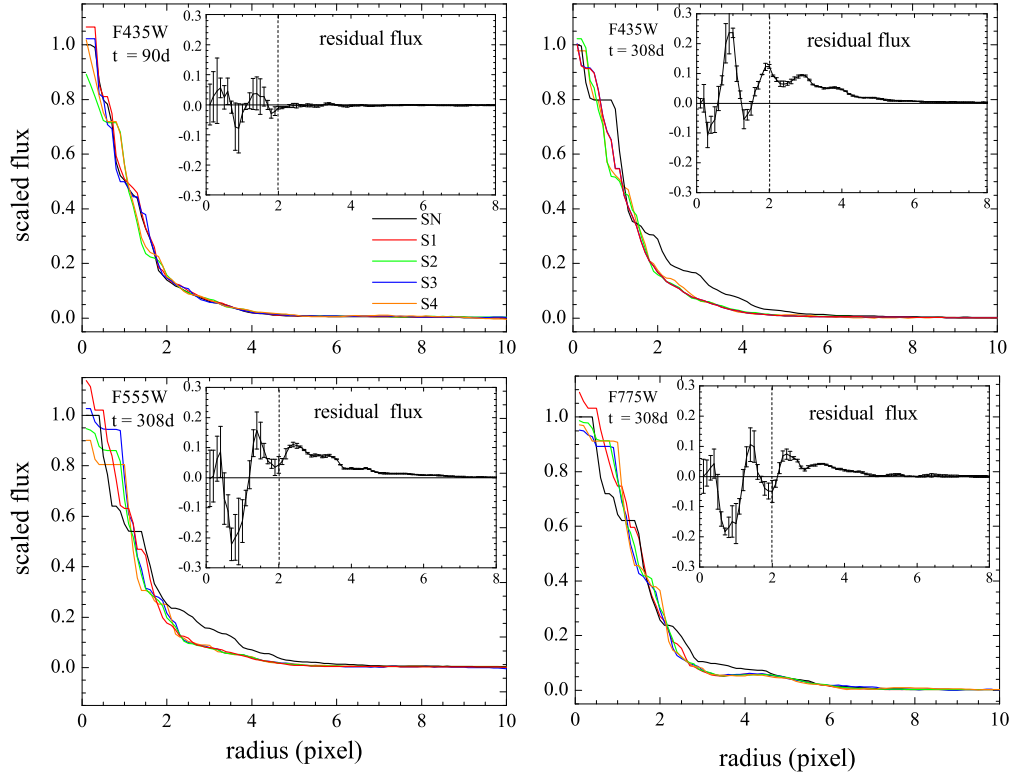


Fig. 3.— Radial brightness profile for SN 2006X in F435W, F555W, and F775W. The black curves show the SN, while the color curves represent local stars in the same field, marked in Figure 1 (S1, red; S2, green; S3, blue; S4, orange). The inset panel shows the residual flux between the SN and the average of the local stars.

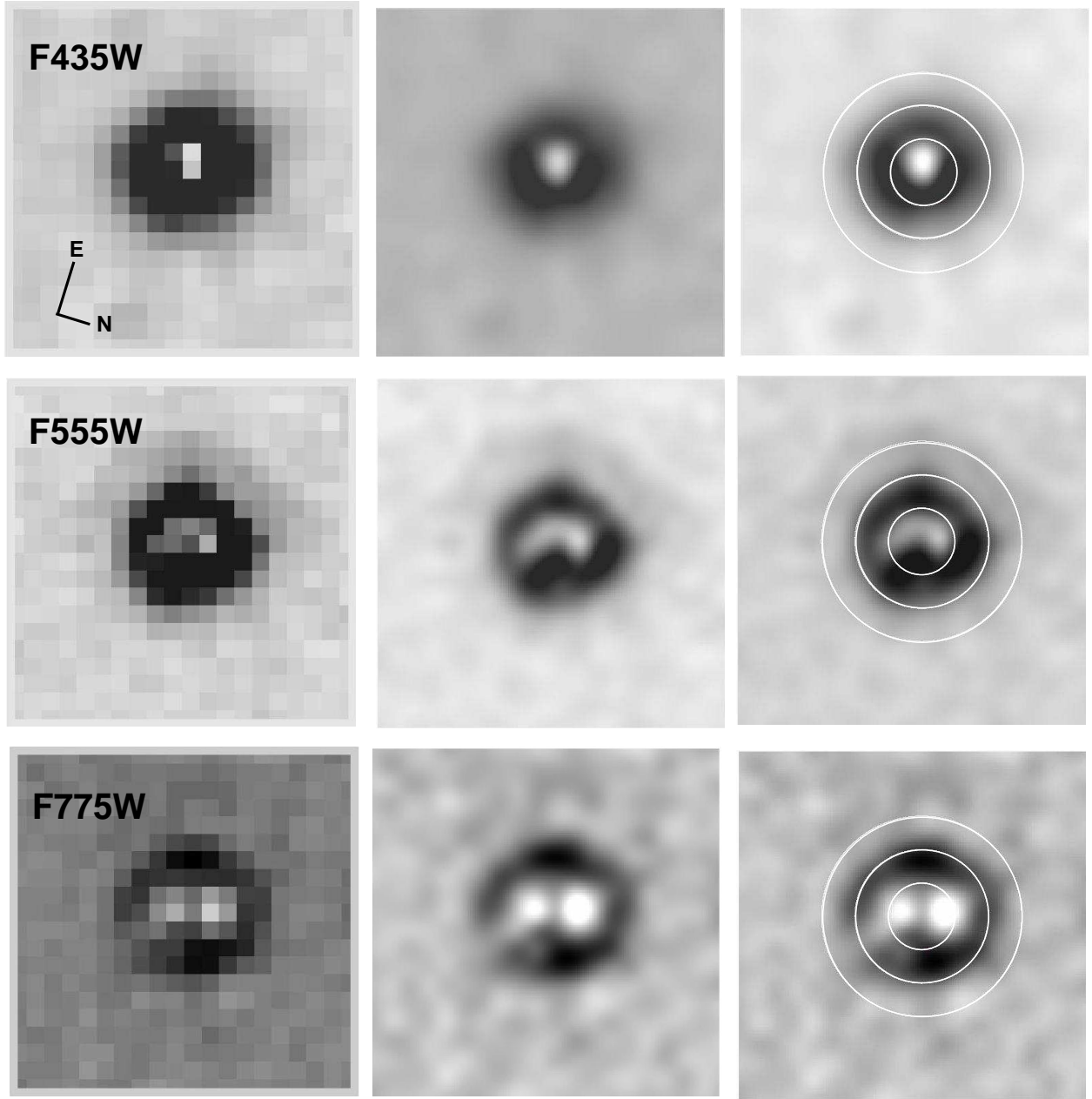


Fig. 4.— The PSF-subtracted *HST*/*ACS* images of SN 2006X (taken on 2006 December 24) with a $0.53'' \times 0.53''$ field surrounding SN 2006X. The supernova is at the center of each frame. Column (1) shows the residual image of SN 2006X obtained by subtracting the local bright Star 1 whose central flux is scaled to that of the supernova; column (2) displays the residual image after resampling from 1 pixel to 8×8 pixels; and in column (3) there are circles of radius 2, 4, and 6 pixels to guide the eye.

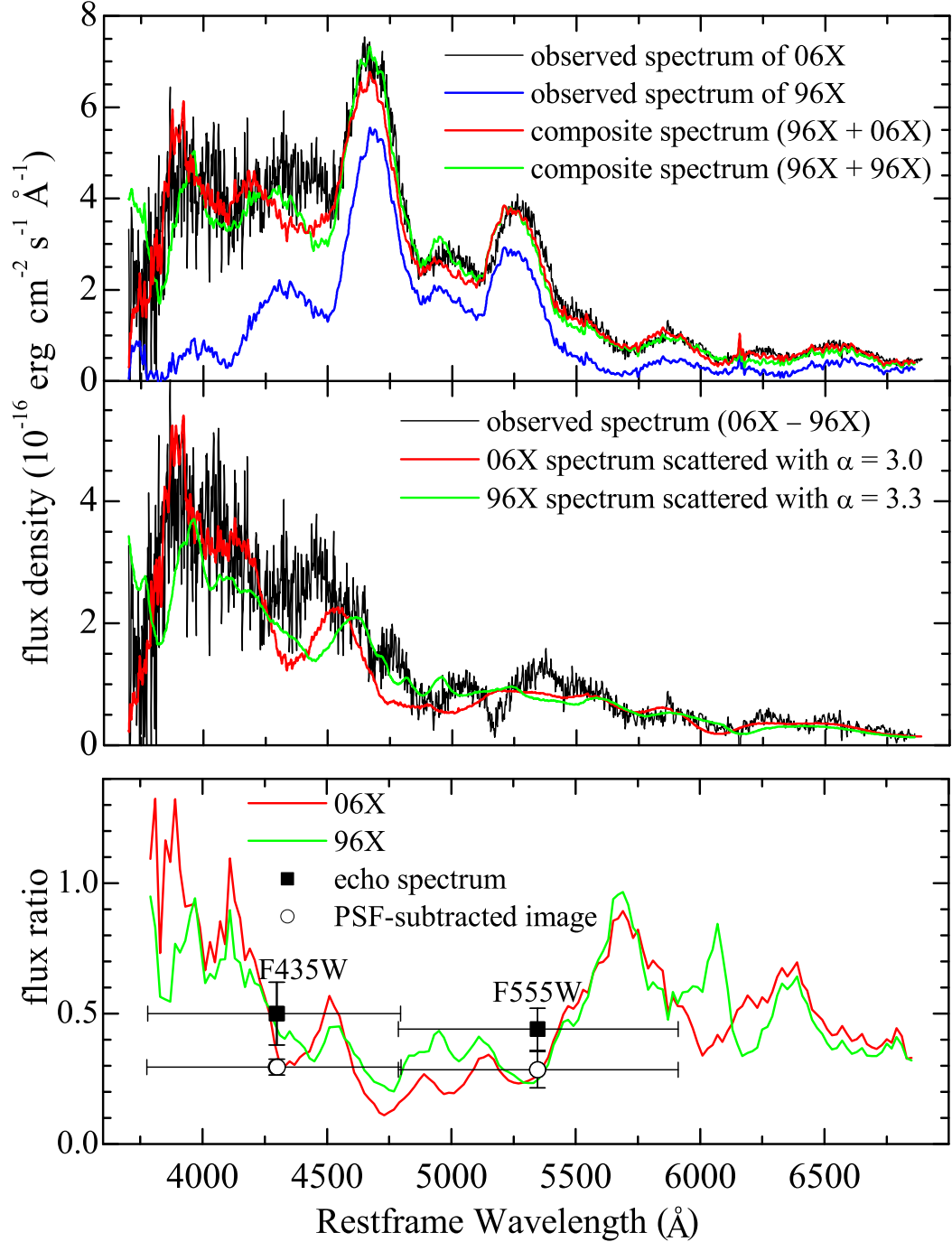


Fig. 5.— Top panel: Comparison of the observed spectrum of SN 2006X at 308 d with the composite spectrum containing the nebular emission of SN 1996X and the emission of the echo computed as described in the text. Middle panel: Residual of the spectral flux between SN 2006X and SN 1996X at $t = 308$ d, overlapped with the time-integrated echo spectra. Bottom panel: The fraction of the total light contributed by the echo as a function of wavelength. The fractions inferred from the PSF-subtracted image (open circles) and the spectrophotometry (filled squares) are also shown with error bars (vertical ones for uncertainties and horizontal ones for the FWHM of the F435W and F555W filters).